Available online at www.eccomasproceedia.org
Eccomas Proceedia SMART (2023) 331-342

ECCOMAS
Proceedia

X ECCOMAS Thematic Conference on Smart Structures and Materials
SMART 2023
D.A. Saravanos, A. Benjeddou, N. Chrysochoidis and T. Theodosiou (Eds)

MORPHING CONCEPT BASED ON THERMOPLASTIC FIBER REINFORCED PLASTICS

Hans van Goozen*, Wouter van der Eijk*, Hermen Pijlman†, Jan Docter†

* GKN Fokker Aerostructures B.V.
Anthony Fokkerweg 4, 3351 NL Papendrecht, The Netherlands
e-mail: fokker.communications@fokker.com, https://www.gknaerospace.com/

† Royal NLR – Netherlands Aerospace Centre
Voorsterweg 31, 8316 PR Marknesse, The Netherlands
e-mail: info@nlr.nl, https://www.nlr.nl/

Abstract: Over the last few decades, much effort has gone into developing compliance-based morphing solutions for reducing drag generated by slots in the wing surfaces required for movables to operate. The main components of these morphing solutions are generally a continuous skin supported by a compliant internal structure. These components should provide sufficient stiffness to resist the aerodynamic loads and, as a contradiction, sufficient flexibility to allow deformation. Against this background, it is investigated whether a novel morphing concept is suitable for a winglet application with a tab to be used for large passenger aircraft wing load alleviation. This concept achieves flexibility and stiffness by combining a carbon fiber-reinforced thermoplastic skin lay-up with glass fiber reinforced thermoplastic so-called shear resistant flexures.

Key words: Morphing, Winglet, Tab, Fiber-reinforced, Thermoplastic, Flexure

1 INTRODUCTION

Several morphing concepts make use of a continuous anisotropic skin in combination with an internally compliant structure driven by actuators. Such anisotropic skins generally consist of a combination of a thin flexible outer skin and a supporting layer made of a corrugated structure or honeycomb. This layer ensures that the outer skin retains its smooth shape under varying aerodynamic pressures and at the same time can take the correct wing shape. The internal compliant structure, to which the anisotropic skin is attached, ensures that the aero loads are absorbed.

The presented novel concept differs in that the skin is made of a laminate supported by discrete shear resistant flexures without the skin and flexures being directly connected. The flexible skin area restricts to a chord width of approximately 100 mm and is able to deform and transfer structural loads at the same time. The flexures have a height restricted to 45 mm and width 80 mm including mounting flanges, and provide the necessary stiffness to withstand the aerodynamic loads while following the deformation of the skin. Figure 1 illustrates this concept:

Peer-review under responsibility of the organizing committee of SMART 2023.
doi: 10.7712/150123.9789.444525

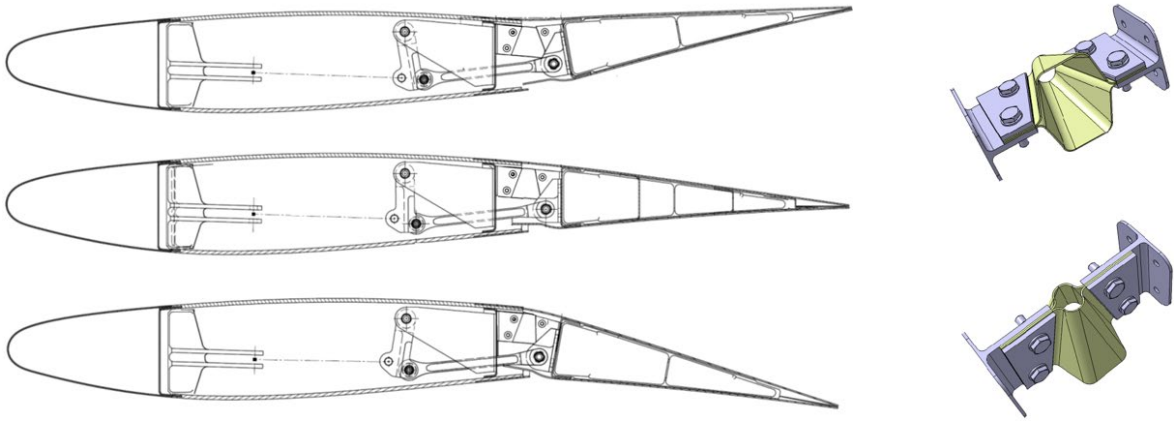

Figure 1: Morphing concept (left) consisting of a flexible skin area with shear resistant flexures (right)

The concept is based on the use of fiber-reinforced thermoplastics, specifically on their toughness and associated flexibility. The skin consist of a C/PPS 6 layered laminate built from 5 Harness Satin weave [1] with a total thickness of 1,86 +0,09 /-0,06 mm. The shear resistant flexures have a tapered cone shape and are stamp formed from 4 layered E-glass/PPS 8 Harness Satin lay-ups [1] having a total thickness of 0,96 ± 0,08 mm.

The current work supports demonstrating that this morphing concept functions as part of a winglet for large passenger aircraft equipped with a tab for wing load alleviation. A representative demonstrator is built for component level testing up to 70% Limit Load (LL). Occurring deformations and strains are predicted by simulation. After component testing, the simulation model will be calibrated to the test data. Simulation with the calibrated model should prove that the morphing parts remains intact up to Ultimate Load (UL). Component testing is done with a novel test-rig concept with springs for applying the aero loads on the morphing tab. Analyses, test and simulations are carried out to study the behavior of the flexible skin and flexures and to prevent failure during component testing.

2 STUDY CASE & REQUIREMENTS

As part of the Clean Sky 2 project MANTA (Movables for Next Generation Aircraft), a study case has been set up in which the winglet of a large passenger aircraft is fitted with a morphing tab to demonstrate that the novel morphing concept works. According to Airbus, the objectives of this tab are to support aircraft functions such as performance improvement (variable camber), load relief (gust, maneuver), roll control and new control such as active suppression of flutter etc. Airbus supplied the aircraft reference geometry, key characteristics, key requirements, the general arrangement and aircraft mission profile [2],[3]. DLR made the aerodynamic design of the baseline winglet loft during the German national project Con.Mov [4]. MANTA introduced a tab including morphing area with a span of 2,13 m and an average chord of 0,55 m, see Figure 2.

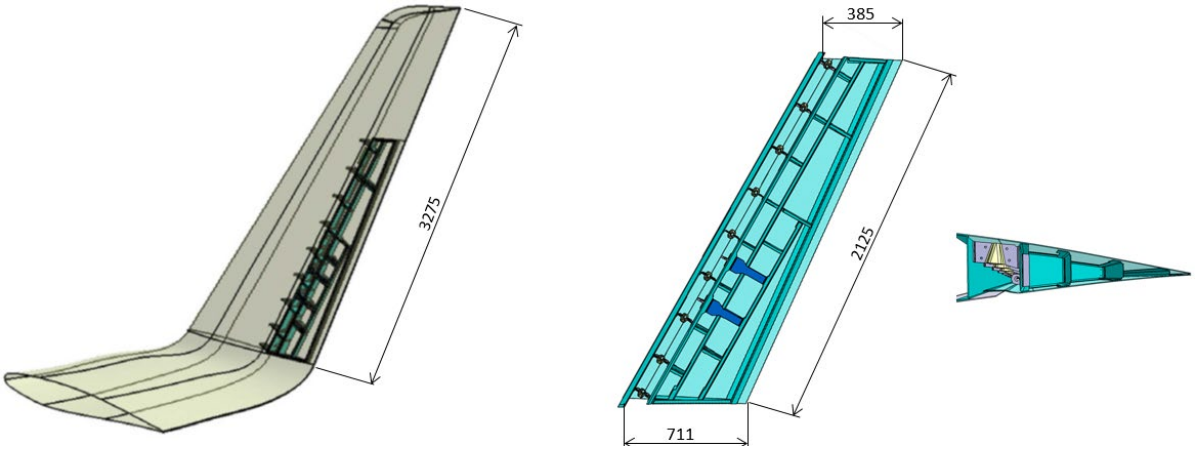

Figure 2: Con.Mov winglet [4] with tab (left) and plan view on tab structure including morphing area (right)

For the study case, LL has been determined for a rudder deflection that produces a sideslip angle of +5° for a high-speed case at Mach 0.85 at 20.000 ft. In combination with a tab angle of +10º, this side slip results in a tab load of 11,95kN in inboard direction [5]. Several load cases have been derived from this LL-case, consisting of combinations of aero load, tab angle, and winglet bending. These load cases cover the expected load spectrum up to including UL.

The contour of the flexible area of the skin forms a circular arc when rotating the tab, which radius decreases with increasing tab angle to a minimum of approximately 500 mm. Within the required tab angle range of $-10° \leq \alpha \leq +10°$, the actual contour must remain within a bandwidth of ±1,0 mm to the nominal circular arc for any tab angle during any load case up to 50% LL, see Figure 3. The novel concept is considered successful if it demonstrates to meet this aerodynamic requirement for the flexible skin surface and that the required actuator loads are at most 10% higher compared to the loads required to actuate the tab if it was fitted with hinges.

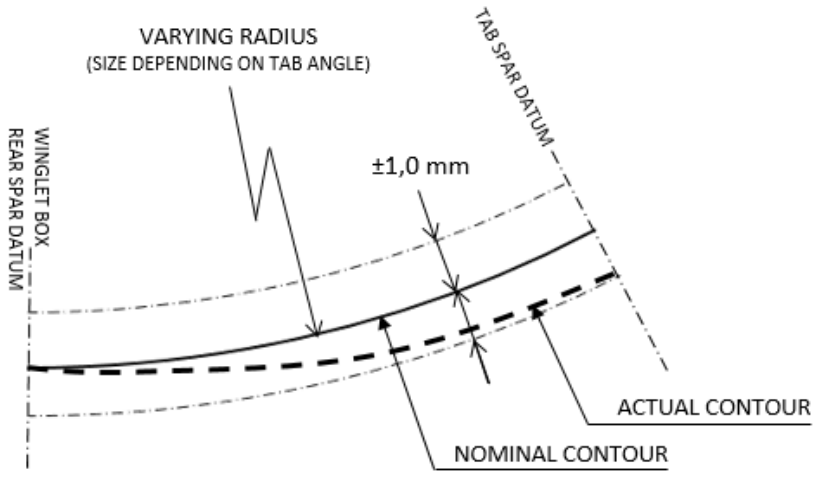

Figure 3: Aerodynamic contour requirement for the flexible skin area [6]

The tab is designed such that buckling of the tab skins does not occur before 70% LL. The flexible area of the inboard tab skin experiences a displacement controlled buckling behavior, which is to be measured during testing at component level.

The design service goal is 28.800 flight cycles or 1.200.000 flight hours. For the flexure, a fatigue spectrum is constructed based on the number and relative magnitude of side load cases of an equivalent aircraft [8], using the maximum load during normal operation and an assumed number of maneuvers.

Its shear stiffness is not allowed to drop more than 10% over its entire service life. After 10% stiffness degradation, one flexure must be able to support a maximum shear load with an absolute value of 675 N, without adverse damage occurring and contour displacements of the flexible skin area not exceeding the requirement of ±1.0 mm for daily operational use. From 50% LL to LL, which is assumed to occur once in the life of the aircraft, one flexure must be able to bear a maximum shear load with an absolute value of 1350 N. Exceeding the contour requirement of ±1,0 mm is allowed provided that no adverse damage occurs. Between LL and UL, the flexure must be able to bear a maximum shear load with an absolute value of 2000 N, while local damage is allowed provided the morphing structure continues to transfer the occurring loads. The shear stiffness should be between 675 N/mm and 2.000 N/mm for all values of the defined tab angle range of $-10° \leq \alpha \leq +10°$. Shear stiffness lower than 675 N/mm leads to exceeding the contour requirement of ±1,0 mm [6].

Keeping the actuator loads within 110% of the load needed to operate the tab with traditional hinges, requires that the chord rotational bending stiffness of the morphing region at sub-component level is not greater than (4200 + 4.7*Ls) Nmm/°. The 4200 part is attributed to the bending stiffness of the flexure of the sub-component. The 4.7*Ls part is attributed to the bending stiffness of the flexible skin with span Ls of approximately 270 mm, which corresponds to the pitch between the nine flexures of the morphing tab component.

3 APPROACH

A technology development plan was made containing the minimum amount of activities to prove that the concept meets the requirements. The structure of this plan is a synthesis between the V&V method, Test Pyramid and technology readiness assessment [8], see Figure 4. The V&V structure is decisive for the division of the concept into product levels, top down from component to coupon/element level. The test pyramid supports the bottom-up interpretation of the type of activities per product level. The link with Technology Readiness Levels (TRL) offers the possibility to implement stage gates to determine whether there is sufficient evidence and conviction to start activities on the next higher product level.

For verification if the requirements for the lower product levels has been met, risk-mitigating tasks are defined. The approach is to carry out analysis, tests and simulations and to optimize the novel concept to the MANTA study case with regard to materials and geometry [9]. Validation whether the concept meets its objectives, takes place through demonstration testing and simulation at component level.

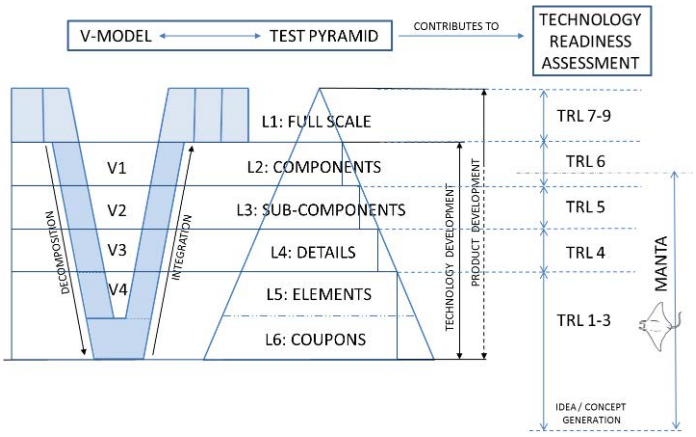

Figure 4: V-model relation scheme [8]

4 BUILDING BLOCK DEVELOPMENTS

The flexible skin area will be loaded repeatedly with high bending strains unusual in aerospace applications. This can lead to damage initiation and growth, which determines the maximum allowed thickness of the flex area that also must provide sufficient buckling resistance at the same time. To verify the fatigue and damage tolerance properties, Four Point Bending Testing (FPBT) at coupon level is applied [10]. For speeding up testing, the amplitude settings corresponds to tab angles ranging from $-34° \leq \alpha \leq +34°$ up to $-65° \leq \alpha \leq +65°$ instead of using the amplitude setting corresponding with the tab angle range requirement. By doing so, it is proven that the fatigue and damage tolerance behavior of a 6-layer C/PPS laminate with a $[\pm 45°, 0/90, \pm 45°]_s$ lay-up provided with Barely Visible Impact Damage (BVID) reaches at least a million cycles. It is also observed that growth of BVID stops after it expands slightly in the direction perpendicular to the bend angle.

Figure 5: Four Point Bending Test [10]

The attachment of the flexible skin by fastening is verified at element level for peel dominated load situations. The used fastener coping with skin thickness is blind bolt EN6122 with a 130° flush head [11]. Static testing results in skin bending failure without affecting the quality of the fasteners, see Figure 6. Fatigue tests show no damage initiation due to fastening and that sample stiffness reduction corresponds with the results of the FPBT [12].

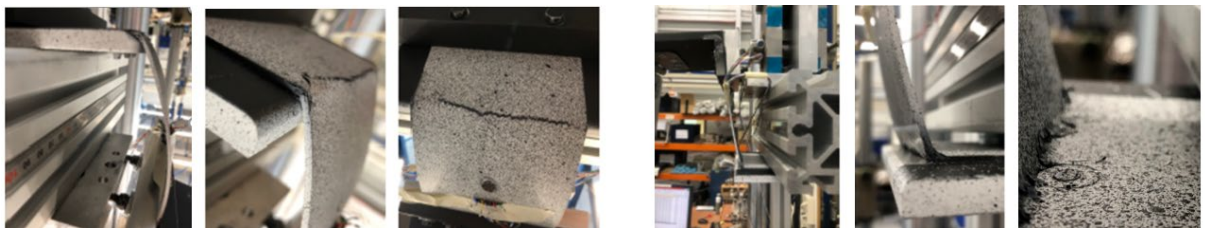

Figure 6: Failure by downward bending at support (left) and upward bending at fastener heads (right)

Characterizing research shows that the baseline flexure inhibits insufficient shear stiffness and that high strains levels result in material failure. The main deformation mechanism of the flexure is folding of the corners during compressive bending and unfolding during tensile bending. Bending tests show that the maximum bending angle that the flexure can obtain without damage initiation is much larger in compressive bending direction than in tensile bending direction. Damage occurs at the compressive side of the corners causing buckled and cracked yarns. Damage to shear loading is found specifically at the top side of the folding corners where compressive forces result in buckled, cracked yarns and delamination [13],[14]. Figure 7 shows the main loading mechanisms and an example of compression damage due to tensile bending.

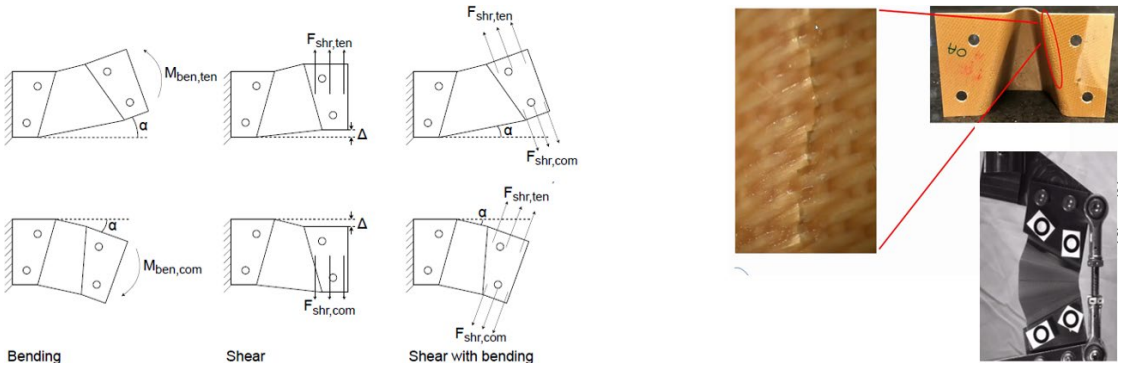

Figure 7: Overview of main loading mechanisms (left) and cracked yarns in outer layers (right)

The current material used, is 8HS E-Glass/PPS, a woven fabric reinforced thermoplastic suitable for hot stamp forming. This material and the process of rubber pressing are qualified for use on the J-noses of the A340 and A380 aircraft. It is concluded to stick with this material because changing from glass to carbon results in a too high stiffness resulting in fiber fracture. Other matrix materials such as Polyaryletherketone (PAEK) are not considered since the bonding properties between these materials and the glass fibers are insufficient. Research into metal as an alternative material will be continued in future.

Folding/unfolding experiments with the baseline material shows that the $[(0,90)]_{2s}$ inhibits the lowest critical corner compression strain levels compared to those of the $[(90,0)]_{2s}$ and $[(45,-45)]_{2s}$, resulting in a lay-up change from $[(45,-45)]_{2s}$ to $[(0,90)]_{2s}$. The processed test data shows that compressive stress levels for this $[(0,90)]_{2s}$ lay-up should not exceed -6000με with less than 10% stiffness reduction [14].

With this knowledge, optimization of the baseline flexure geometry aims at increasing the shear stiffness while remaining bending compliant without exceeding the critical strain limit. Therefore, the behavior is modeled with FEM and a design tool is developed for determining the optimum geometry of the flexure with the stress requirements as input extended with the requirements regarding maximum allowed strain level and layer orientations [14]. Changes resulting from using the design tool are increased height (H), decreased clamp width (CW), increased angle α, and removal of the mid area face, see Figure 8. The number of shells per flexure increased from two to four.

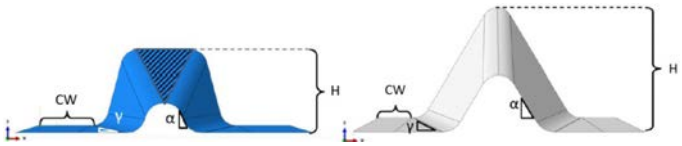

Figure 8: Baseline geometry (left) and optimized flexure geometry (right)

Figure 9 shows the strain levels in the bottom plies of the baseline flexure and optimized flexure under tensile bending and tensile bending combined with shear. The boxes around the strain values are colored red when the critical strain of -0.006με is exceeded.

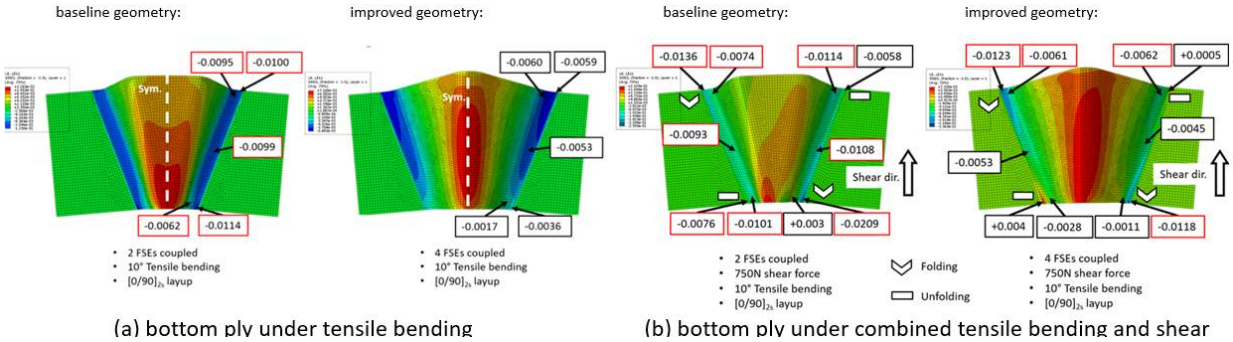

Figure 9: Strain level overviews of bottom ply [15]

Table 1 compares the values for shear, flexure, and compression between the test results of the baseline geometry and the FE-modeling values of the optimized geometry against the requirements:

Table 1: Requirements and values determined for the baseline and improved flexures [15]

	Min. Shear stiffness [N/mm]	Max. bending stiffness [Nmm/°]	Max. compression strain at middle of fillet in bottom ply under tension bending combined with shear [µm]
Requirement	>750	<4200	<6000
Baseline flexure	941	2290	9300
Improved flexure *)	1409	1417	5300

*) values are based on application of four shells per flexure

5 SIMULATION AND DEMONSTRATION

The test program for demonstration is divided into two stages: one for physical testing to 70% LL, and one for simulation of the functioning of the morphing concept to 1,5x LL. The simulation is based on FE-modeling that must be calibrated with the physical test data [16]. A tab component is built that is subjected to the set of load cases derived from LL consisting of combinations of tab air loads, winglet-bending curves and tab angles, see Figure 10.

Tab rotation [°]	Limit Load [%]						
	70	50	25	0	-25	-50	-52,5
10	LC-16	LC-37		LC-4		LC-33	
		LC-3		LC-44			
		LC-35		LC-48			
5	LC-22		LC-38	LC-24			
			LC-41	LC-45			
			LC-53	LC-49			
0	LC-18						LC-19
				LC- 42			
				LC-50			
-5				LC-29	LC-39		LC-27
				LC-46	LC-43		
				LC-51	LC-54		
-10		LC-36		LC-14		LC-40	LC-17
				LC-47		LC-55	
				LC-52		LC-34	

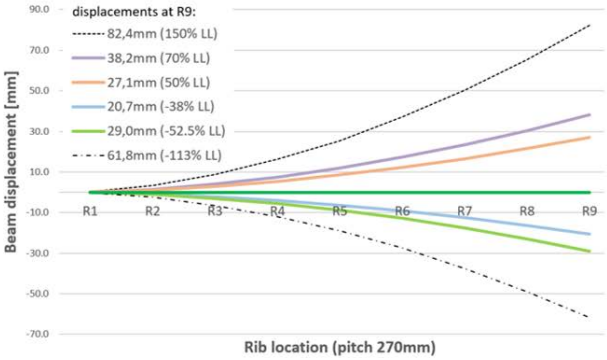

Figure 10: Load cases for physical testing (left) and winglet bending curves (right)

The tab component consists of a frame of light alloy sheet spars and ribs provided with C/PPS skins at both sides. The ribs have a pitch of approximately 270 mm and determine the positions of the nine shear resistant flexures. Two NC-machined ribs introduce the actuator loads for setting the tab angles, see Figure 2. Deformations and strains have been predicted with a simulation model based on the winglet and tab design, making use of the structural characteristics provided by the research at the lower product levels. Figure 11 shows this model for the LL-case in which the deformation of the flexible area of the skin is clearly visible.

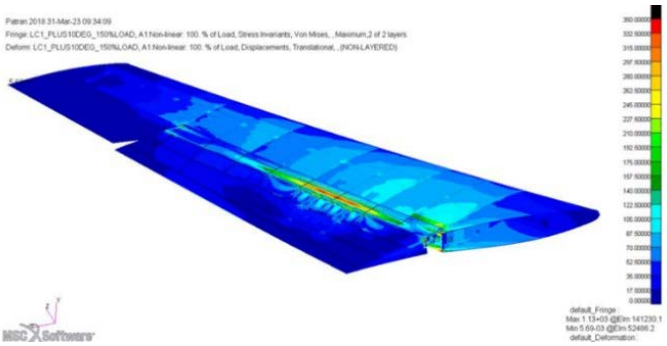

Figure 11: FE-model containing winglet and tab structure

In order to match the FE-model to the test set-up, the structure of the winglet box is replaced by a test beam, which is subjected to bending during testing. The beam is stiffened such, that its bending curves fits those of the winglet box. The flexible skin and flexures forming the morphing area are attached to this test beam, see Figure 12.

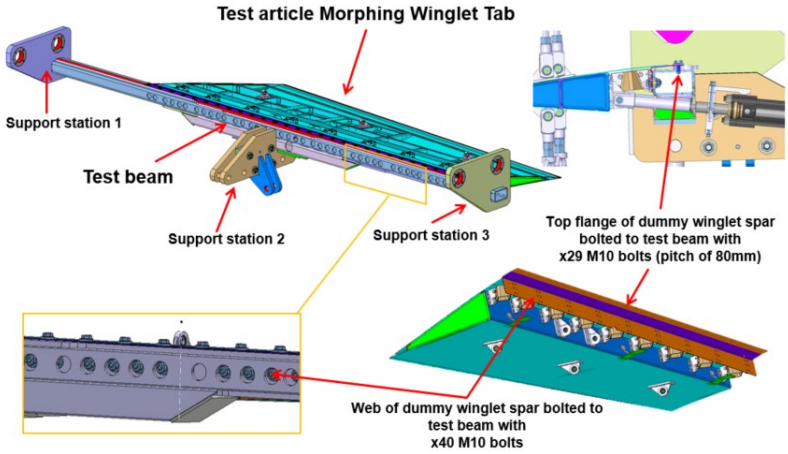

Figure 12: Demonstrator attached to test beam

The test setup developed for demonstration exists of a rig frame and load introduction devices to which the assembly of test beam and morphing tab is installed, see Figure 13. During demonstration, the deformations of the flexible skin area, strains in the shear resistant flexures, imposed loads and reaction forces are measured. The data retrieved is used for verification of the predicted deformations and strain levels and for calibration of the simulation model.

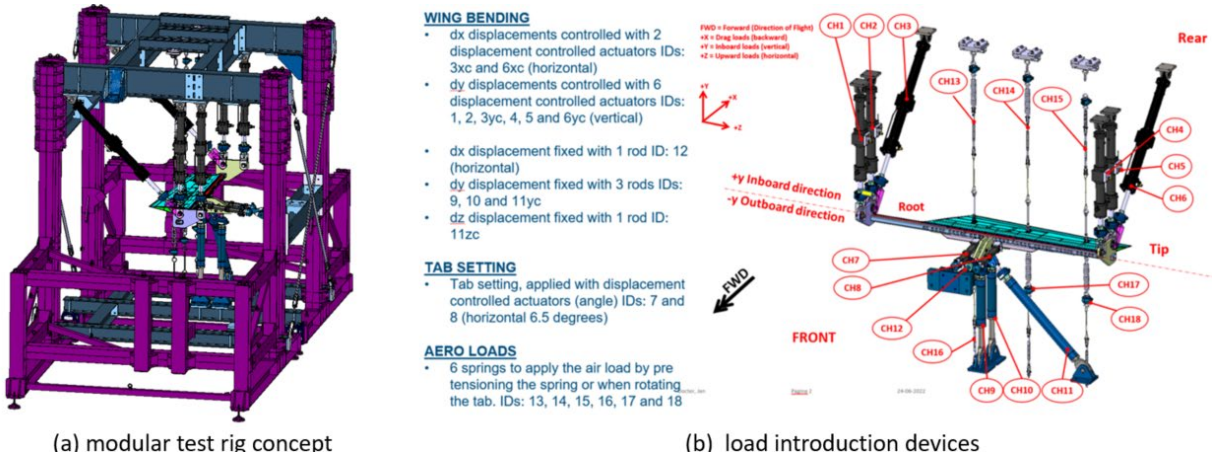

(a) modular test rig concept (b) load introduction devices

Figure 13: MANTA modular test rig with morphing winglet tab demonstrator

The rig frame is modular to accommodate testing of various movable systems. The rig is sized to internally transfer the loads between the active and passive load introduction devices. Because the actuators are displacement controlled, the rig is stiffened to minimize deformations at the actuator and strut connections. To be able to execute static and dynamic load cases for the morphing concept demonstration, the test rig realizes variation of tab setting, inducement of aerodynamic loads on the tab, and inducement of test beam bending curvature. Two displacement-controlled actuators control the tab angle positions. The aerodynamic loads are

applied on three fixed locations on the outboard skin and the inboard skin by using dedicated springs. Each spring load train has a load-measuring device.

As shown by Figure 13, the test setup consists of three stations for deforming the test beam. The outer stations are displacement controlled by actuators and the inner station at the tab actuation position is constraint by four load measuring struts.

The outer shells of the flexures are equipped with strain gauges at each flexure position. For setting the tab angle, a Digital Image Correlation (DIC) system measures two points at the rib position in between the two tab deployment actuators. It also measures the resulting tab angles at the other rib positions, the displacements of the flexible skin area, and the bending curve of the test beam. Figure 14 shows the measurement instrumentation.

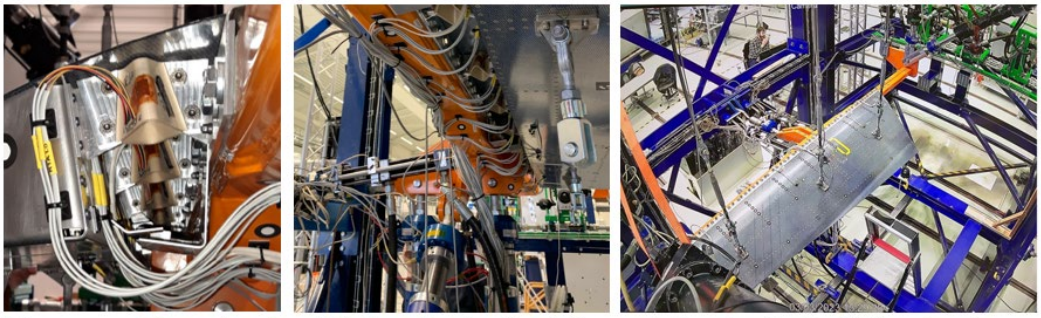

(a) flexure assemblies equipped with strain gauges

(b) bottom view showing strain gauge wiring

(c) top view showing DIC laser targets for displacement measurement

Figure 14: Measurement instrumentation

6 RESULTS AND CONCLUSION

At the time of compiling this document, the static tests up to 70% LL are completed at component level, however, analysis of strain and displacement data remained limited to assessing the measured displacements. The following summarizes the main findings so far:

No significant deviations or unexpected behavior occurred; visual inspection of the flexible skin area and shear resistant flexures shows no damage. Angular deviations have been measured when imposing aero loads; at an aero load of 50% LL, the angular offset on the nominal tab angle is 0,8° maximum. The tab actuator loads remain within the requirement of not exceeding 110% of the loads needed for actuating the tab if fitted with conventional hinges.

During the load cases representing normal operational use, 95% of the contour measurements of the flexible skin area remain within the required band width of ±1,0 mm, with gradual transitions between the flexible area and the fixed skin. Most contour deviations occur during -10° inboard tab rotation combined with tab loads and winglet bending both directed outboard. For example, for the combination of a tab angle of -10°, tab load of 50% LL and winglet deflection of 27,2 mm (LC55, Figure 11), the contour of the flexible area lies partially outside the bandwidth of ±1,0mm. Figure 15 illustrates this. In this figure, the neutral contour is the measured contour without aero loads and without winglet bending. The measurements were made over a length of 120 mm, with the fastener rows that border the flexible area on either side as starting and ending points.

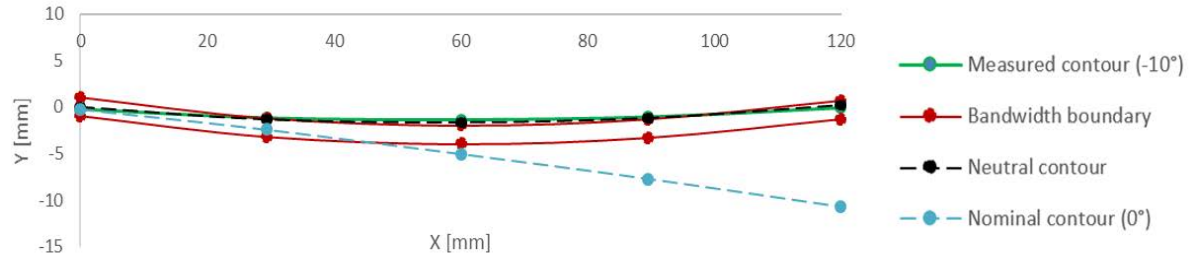

Figure 15: Flexible skin area contour for LC55

For the load cases at 70% LL, the contour remains relatively smooth without any sharp transitions from the fixed skin to the flexible area. The displacement-forced buckling behavior of the flexible area as predicted by the simulation (see Figure 11) has been confirmed by testing; Figure 16 shows the data of the largest contour deviation measured at the rib positioned in between the actuator load introduction ribs (see Figure 2). This concerns data recorded at a tab angle of +10° combined with a tab load of 70% LL and winglet deflection of 38.2 mm both in inboard direction (LC16 acc. to Figure 10).

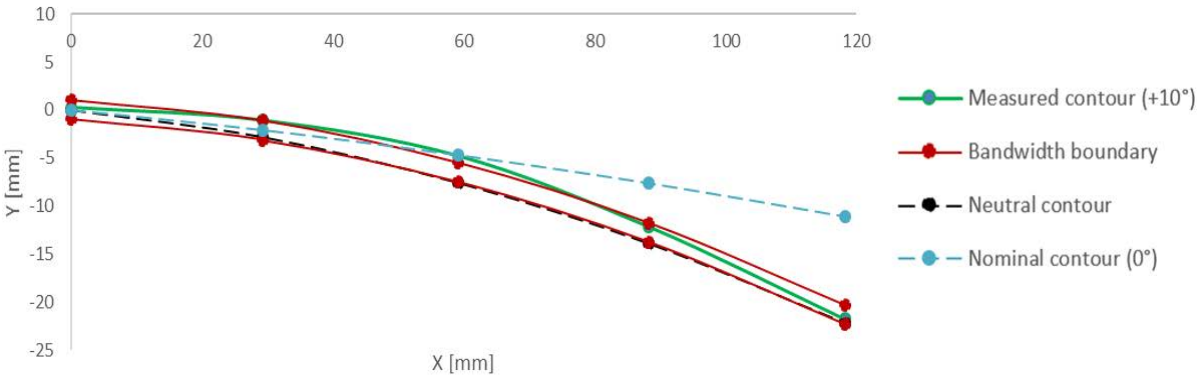

Figure 16: Displacement-forced buckling of the flex area at rib 4 (LC16)

Although analyses has limited to displacement measurement data so far, it can be concluded that the novel morphing concept functions up to 70% LL as part of the winglet with tab defined by the MANTA study case. The 5% of the contour measurement data of the flexible skin area that is outside the required band width of ±1,0 mm requires further evaluation and investigation, as do the angular offsets on the nominal tab angle settings that occur when imposing aero loads.

9 ACKNOWLEDGEMENTS

Clean Sky 2 funded this research under Grant Agreement number 724558, as part of European Union's Horizon 2020 research and innovation programme.

The authors would like to thank Airbus and DLR for their input at aircraft level, University of Twente for performing the lower product level developments as partner of the AEROMO2 consortium, and TUD for determining the LL case.

10 REFERENCES

[1] Toray Advanced Composites, “Cetex® TC100 – Datasheet,” www.toraytac.com, 2021.

[2] A. Eberle, “Delivery of XRF-1 CAD geometry,” Coordination Memorandum-MANTA-2017-1, Airbus,” 2017.

[3] A. Eberle, “Specifications and design assumptions for XRF1 target application outer-wing,” Airbus, 2018.

[4] Y. M. Meddaikar, “DLR-XRF1-C (with winglet) Model Delivery for MANTA,” DLR, 2019.

[5] P. Lancelot, “MANTA – WP4 Aerodynamic load analyses for the control surfaces ground demonstrators,” TUD, Delft, The Netherlands, Tech. Report AIR-A-4.1.2.6, 27 Nov. 2020.

[6] H. van Goozen, W van der Eijk, “Lower V-level requirements for the WMT development,” GKN Fokker Aerostructures, Papendrecht, The Netherlands, Tech. Report TYG03-WP4-REP-210114, 25 Nov. 2021.

[7] Federal Aviation Agency, *Statistical loads data for the Boeing 777-200ER aircraft in commercial operations*, Washington, DC: Office of Aviation Research and Development, 2006.

[8] H. van Goozen, “MANTA - Generic Development Plan,” GKN Fokker Aerostructures, Papendrecht, The Netherlands, Tech. Report KO-A-4.1 .2.3-1, 6 Dec. 2017.

[9] H. van Goozen, “MANTA - Development plan for winglet with morphing tab,” GKN Fokker Aerostructures, Papendrecht, The Netherlands, Tech. Report AIR-3-FAE-DEL-0001, 30 Jan. 2020.

[10] A. van Eemeren, “F&DT of a 6-layer C/PPS laminate under pure bending after impact,” GKN Fokker Aerostructures, Papendrecht, The Netherlands, Tech. Report TYG03-WP4-REP-200604, 21 Aug. 2020.

[11] “Aerospace series blind bolt 130° flush head high strength, preferable in composite application,” prEN6122:2005, European Association of Aerospace Industries Standardization, Brussels, Belgium, Apr. 2005.

[12] A. van Eemeren, “Joint development for a morphing skin,” MS Thesis, Delft University of Technology, Delft, The Netherlands, 2021.

[13] T.J. van Rijnsoever, “Characterization of a flexible shear element used in a morphing winglet concept,” MS thesis, University of Twente, Enschede, The Netherlands, 2021.

[14] M.J. Materman, S. Benou, L.L. Warnet and R.D.R. Sitohang, “Design methodology of a shear resistant flexure for a morphing structure,” presented at 10th ECCOMAS Thematic Conference on Smart Structures and Materials, Patras, Greece, 2023.

[15] H. van Goozen, W. van der Eijk, L.L. Warnet, R. Haagsma, J. Docter and J. Vroon, “Final technical design description demo #1 (Winglet Morphing Tab),” GKN Fokker Aerostructures, Papendrecht, The Netherlands, Tech. Report KO-A-4.1.2.4-1, 23 Aug. 2022,

[16] H. van Goozen, W van der Eijk, “V1-level Test Specification for the WMT Demonstrator,” GKN Fokker Aerostructures, Papendrecht, The Netherlands, Tech. Report TYG03-WP4-REP-210917, 12 Apr. 2021.